PCCP

Accepted Manuscript

This is an *Accepted Manuscript*, which has been through the Royal Society of Chemistry peer review process and has been accepted for publication.

Accepted Manuscripts are published online shortly after acceptance, before technical editing, formatting and proof reading. Using this free service, authors can make their results available to the community, in citable form, before we publish the edited article. We will replace this *Accepted Manuscript* with the edited and formatted *Advance Article* as soon as it is available.

You can find more information about *Accepted Manuscripts* in the Information for Authors.

Please note that technical editing may introduce minor changes to the text and/or graphics, which may alter content. The journal's standard Terms & Conditions and the Ethical guidelines still apply. In no event shall the Royal Society of Chemistry be held responsible for any errors or omissions in this *Accepted Manuscript* or any consequences arising from the use of any information it contains.

ROYAL SOCIETY OF CHEMISTRY

www.rsc.org/pccp

PCCP RSCPublishing

PAPER

Catalytic etching of monolayer graphene at low temperature *via* carbon oxidation

Cite this: DOI: 10.1039/x0xx00000x

Received 00th January 2012, Accepted 00th January 2012

DOI: 10.1039/x0xx00000x

www.rsc.org/

Jun Eon Jin,[a] Jae-Hyun Lee,[b] Jun Hee Choi,[a] Ho-Kyun Jang,[a] Junhong Na,[a] Dongmok Whang,[b] Do-Hyun Kim,*[a] Gyu Tae Kim*[a]

In this work, an easy method to etch monolayer graphene is shown by using catalytic oxidation in the presence of ZnO nanoparticles (NPs). The catalytic etching of monolayer graphene, which was transferred to the channel of field-effect transistors (FETs), was performed at low temperature by heating the FETs several times under inert gas atmosphere ($ZnO + C \rightarrow Zn + CO$ or CO_2). As etching process proceeded, diverse etched structures in the shape of nano-channels and pits were observed in microscopic observation. To confirm the evolution of etching, current-voltage characteristics of monolayer graphene were measured after every step of etching by catalytic oxidation. As a result, the conductance of monolayer graphene decreased with the development of etched structures. This decrease in conductance was analyzed by percolation theory in honeycomb structure. Finally, well-patterned graphene was obtained by oxidizing graphene under air in the presence of NPs, where Al was deposited on graphene as a mask for designed patterns. This method can substitute graphene etching *via* carbon hydrogenation using H_2 at high temperature.

Introduction

Graphene, single-atom-thick carbon layer of honeycomb lattice, has attracted an attention since its discovery in 2004 due to the unique properties such as transparency, flexibility, mechanical strength, good thermal conductivity and high mobility.[1-6] Especially, graphene is used in the fields of organic solar cells, light emitting diodes, and wearable devices[7-12] on account of its outstanding electrical properties. However, in spite of the excellent electrical properties, a technical barrier exists in the application to electronics because it is a semiconducting material with zero band gap. For this reason, much effort has been made to modify the electronic structure theoretically and experimentally for further application. Theoretical studies revealed that vacancy defects play a role in tuning the electrical structure and magnetic properties of graphene.[13,14] In addition, to open band gap, experimental works have reported several methods to modulate the electrical properties by metal doping, nano-ribbon, ripple, and nano-mesh fabrication.[15-19] Particularly, the method of obtaining graphene in nano-size has attracted an attention due to a change in the electrical properties. Theoretical and experimental studies revealed that graphene nanoribbon can be obtained via unzipping CNT by using transition metal catalyst.[20-22] Also, it has been pointed out in theoretical and experimental studies that graphene nanoribbon can be successfully synthesized from oxidized graphene.[23,24]

Among diverse approaches to modify the structure and electrical properties, catalytic hydrogenation of carbon has been interested as a method to etch graphene sheet.[25-28] In this method, Fe and Ni nanoparticles (NPs) are deposited on graphene layer as a catalyst, and the graphene with NPs is heated at high temperature (700-900 °C) under hydrogen atmosphere. Then, the catalysts produce methane gas *via* catalytic reaction between C and H_2 while moving around the layer of graphene ($C + 2H_2 \rightarrow CH_4$). As a result of the catalytic reaction by catalyst NPs, graphene sheet is cut into pieces and leads to etched nano-structures such as a channel and an island in nano-scale. Also, there were previous reports on etching graphene layers by using non-transition metal oxides such as SiO_x and TiO_2.[29,30] However, these methods inevitably use H_2 at high temperature to etch graphene, or a specific light source matched with the band energy of photocatalyst like TiO_2. It results in a technical barrier in cost and safety aspects. Oxygen plasma etching can be an alternative way to etch graphene easily. But, this method requires expensive equipment and is not suitable for mass production. This situation motivated us to suggest an alternative way to etch graphene at mild conditions *via* catalytic reaction.

Physical Chemistry Chemical Physics Accepted Manuscript

This journal is © The Royal Society of Chemistry 2013

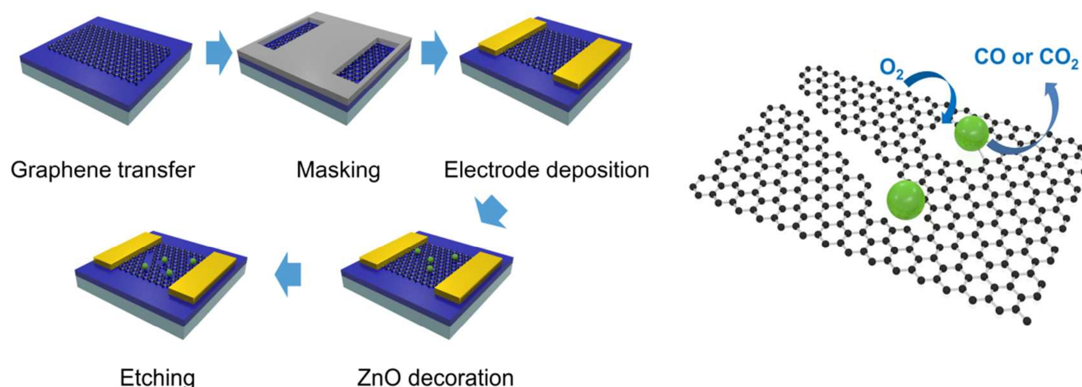

Fig. 1 Schematic diagrams of etching graphene on FET. Graphene is etched at 250 °C under Ar atmosphere by the solid-state reaction between ZnO and C (oxidation: ZnO + C → Zn + CO or CO_2, reduction: Zn + $1/2O_2$ → ZnO).

This study shows that carbon gasification which is a simple process of carbon oxidation can etch graphene at low temperature under air and Ar atmosphere. The main idea is to etch graphene by converting C to CO or CO_2 by using the C + O_2 reaction, where transition metal oxide (TMO) is used as a catalyst to etch graphene. The previous works reported that TMO worked as a catalyst in carbon oxidation.[31,32] Furthermore, several studies demonstrated that porous multi-walled carbon nanotubes (MWCNTs) can be producible by using carbon oxidation in the presence of TMO catalyst.[33-35] In this study, ZnO was selected as a catalyst to etch graphene by gasifying carbon *via* the solid-state reaction (C + O_2 → CO or CO_2). It is because ZnO is also one of TMOs which have catalytic activity toward carbon.[36] ZnO was prepared from $Zn(NO_3)_2 \cdot 6H_2O$ by decomposing the precursor to ZnO on graphene. After ZnO decoration, graphene was heated to create C vacancies by carbon gasification *via* ZnO NPs. The solid-state reaction between graphene and NPs led to etched structures such as a channel and a pit in nano-scale. Furthermore, this catalytic oxidation was carried out at low temperature in air (250 °C) and even under inert gas atmosphere (300 °C), which is the first example to etch graphene at low temperature without using H_2 to the best of our knowledge.

With the etching technique at low temperature, this study also put emphasis on how the presence of TMO NPs influences the morphological change of graphene sheet under inert gas atmosphere. It is significant because graphene is usually synthesized on Ni foil and transferred to other substrates. A small amount of Ni on graphene could contribute to modulate the electronic structure of graphene by introducing vacancies *via* heat treatment like annealing. To show the impact of TMO NPs, the etching of monolayer graphene was conducted under Ar atmosphere in the presence of a catalyst.

Etching process was performed on monolayer graphene transferred to the channel of field-effect transistors (FETs) to prove the evolution of etched structures through a change in current characteristics. Fig. 1 exhibits the schematic process of etching monolayer graphene under Ar atmosphere. FETs were fabricated by using graphene and the solution of Zn precursor was dropped in the channel of FETs. Then, graphene in the channel of FETs was decorated with ZnO by heating the devices at 250 °C for 2 h under Ar atmosphere and the devices were exposed to air for one night under atmospheric conditions. Next, the FETs were heated under the same conditions (250 °C, 2 h, Ar) to etch monolayer graphene (ZnO + C → Zn + CO or CO_2) and exposed to air repeatedly (Zn + $1/2O_2$ → ZnO). These processes were repeatedly conducted under the same experimental conditions to develop the etched structure further.

The structure of monolayer graphene is exactly same to the honeycomb structure. Thus, graphene etching means a partial destroy of the honeycomb structure of graphene, leading to the decrease in the conductance of graphene. This phenomenon is corresponding to the two dimensional percolation in honeycomb lattice. Hence, the change of electrical properties by the vacancy creation in graphene can be analysed by bond percolation theory in honeycomb structure. Up to now, few efforts have been made to clarify if the evolution of vacancy in graphene obeys the two dimensional percolation theory of honeycomb lattice. FET is employed to collect the conductivity of etched graphene for percolation analysis in sp^2 carbon networks as well as to prove the effect of etching graphene indirectly. By using data measured from FET, we report C-C bonding percolation in graphene.

Finally, patterning was realized easily by using carbon gasification under air atmosphere at low temperature. This carbon gasification can substitute carbon hydrogenation reaction where graphene is etched by catalytic reaction at high temperature under H_2 atmosphere.

Results and discussion

Effect of catalytic etching on monolayer graphene

 This journal is © The Royal Society of Chemistry 2012

Physical Chemistry Chemical Physics Accepted Manuscript

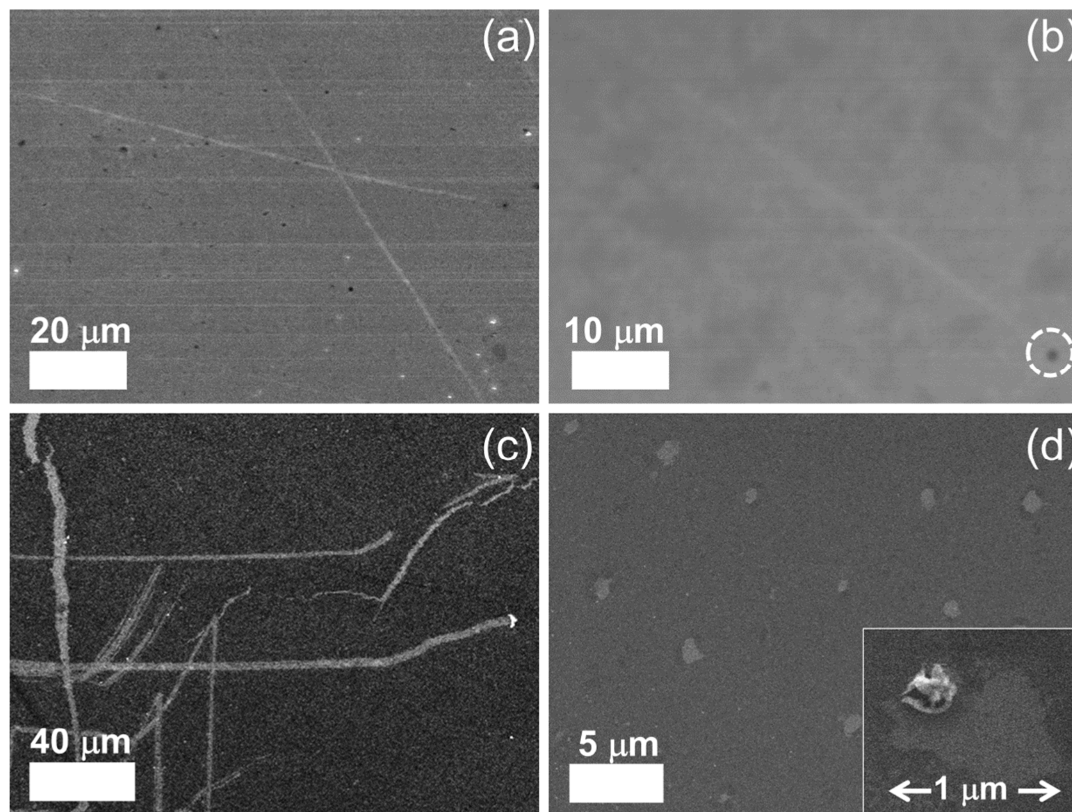

Fig. 2 SEM images of etched graphene by ZnO. The structures in the shape of a channel (a, b, and c) and a pit (d) appear after etching process. ZnO NPs are located at the end of the etched channel or inside a pit (see inset). Various channels with different widths are created on graphene, depending on the diameter of ZnO NPs.

To see the effect of density of NPs on etching, we prepared two concentrations (1 and 8 mM) of Zn precursor solutions. After the whole etching processes were completed by using each solution under Ar atmosphere, the etched structures on monolayer graphene were investigated by using scanning electron microscopy (SEM) as shown in Fig. 2. The figure shows that multi-carbon vacancies are created in the shape of channels and pits after etching monolayer graphene sheet. Fig. 2(a) displays a few channels etched by low concentration of precursor solution. The channel width is approximately 650 nm and the shape of the channel is a straight line crossing each other. This is exactly the same etched structure reported on graphene etching by using carbon hydrogenation ($C + 2H_2 \rightarrow CH_4$).[25-28] Fig. 2(b) shows another etched channel which exists solely in graphene. The channel width was measured to be 600 nm. Interestingly, we can see a NP (indicated with a dashed circle) at the end of the etched channel. It can be deduced that the NP contributed to the creation of one channel *via* catalytic reaction. Meanwhile, Fig. 2(c) exhibits a lot of etched channels created by high concentration of the precursor solution. Different from Fig. 2 (a) and (b), wider channels have been formed in an irregular pattern. However, we can also see that bigger NP is present at the end of the etched channel, and the phenomenon is in good agreement to the result shown in Fig. 2(b). It is thought that the high concentrati-on solution resulted in agglomerated NPs which led to wide channel. Fig. 2(d) exhibits a different shape of the etched structure from the channel where high concentration of solution was used for etching. Various diameters of pits are observed on etched graphene, and the diameter ranges from 400 nm to 1 μm. The vacancies in the etched channels are apparent evidence of missing C atoms of graphene sheet. This clearly indicates that graphene was etched by carbon gasification *via* decorated particles ($ZnO + C \rightarrow Zn + CO$ or CO_2), leading to multi-carbon vacancies. Also, this surely comes to the conclusion that the etched structures of a pit were formed by ZnO NPs during annealing for the solid-state reaction between ZnO and C. These results are consistent with previous work reporting that reduction of NiO by C cut MWCNTs into pieces ($NiO + C \rightarrow Ni + CO$ or CO_2).[31] However, in this case, the solid-state reaction between NiO and C occurred at 900 °C which is much higher than the temperature (250 °C) in this work. For the reduced Zn NPs to etch graphene continuously, we exposed the etched sample to the air for one night (oxidation: $Zn + 1/2O_2 \rightarrow ZnO$).

For a specific analysis about the shape of etched structures and NPs, atomic force microscopy (AFM) analysis was performed on the fully etched monolayer graphene by using high concentration solution. Similar to the images obtained in SEM fully analysis, graphene sheet was randomly

Physical Chemistry Chemical Physics Accepted Manuscript

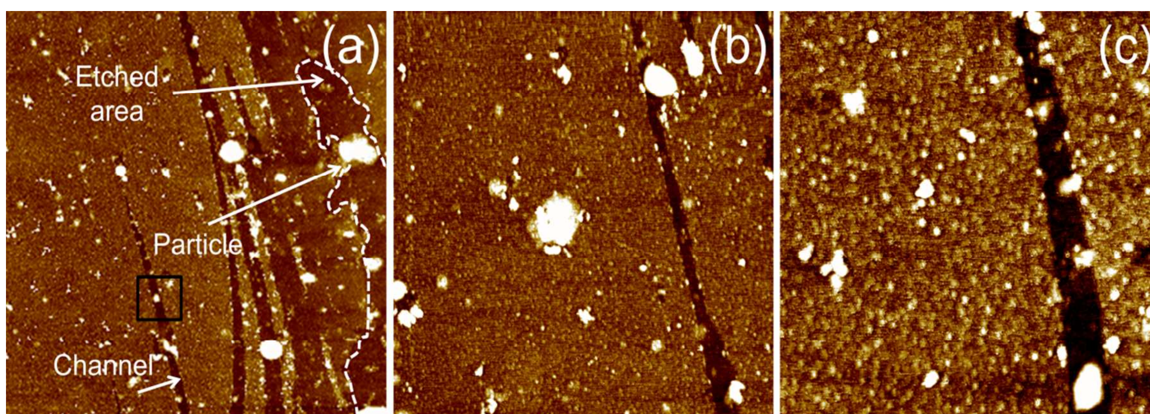

Fig. 3 AFM images of fully etched graphene: (a) 10 μm × 10 μm, (b) 5 μm × 5 μm, and (c) 2.5 μm × 2.5 μm. As shown in (a), channels gradually become narrow toward the end with the presence of NPs. This strongly means that the channel was created by ZnO NPs *via* carbon gasification.

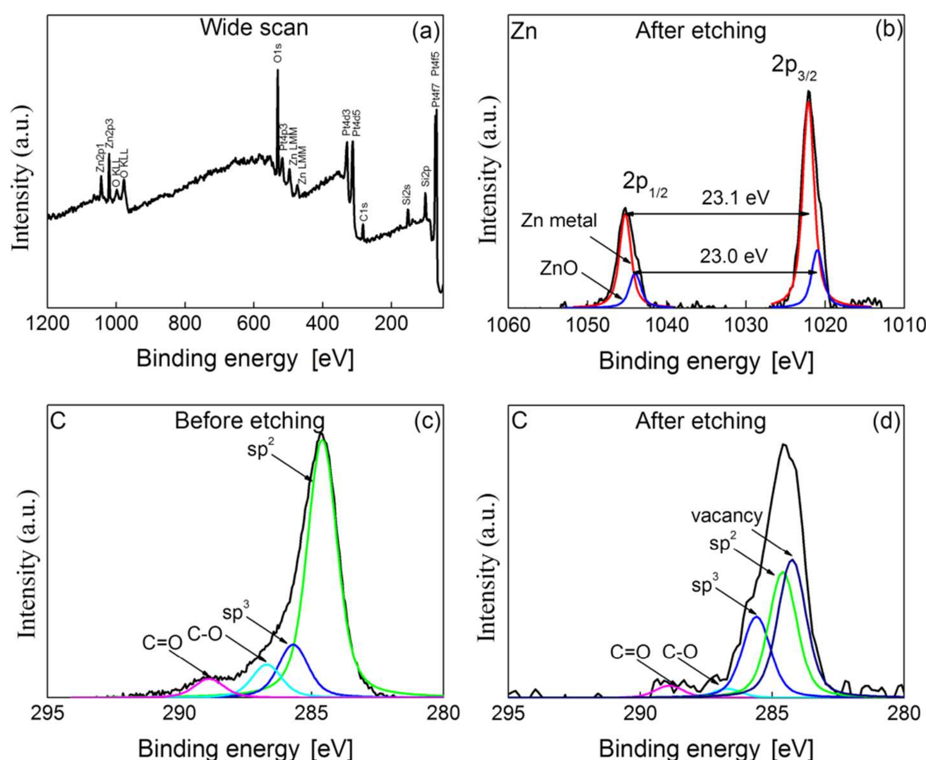

Fig. 4 XPS spectra measured from pristine and etched graphene: (a) wide scan obtained from the fully etched graphene by ZnO, (b) the core level spectra of Zn 2p after etching graphene, and the core level spectra of C 1s from (c) pristine graphene and (d) etched graphene.

etched by the solid-state reaction between graphene and catalyst NPs. The graphene in Fig. 3(a) is decorated with ZnO NPs, where some NPs are located at the edge of etched structures. This becomes clear at the magnified AFM images displayed in Fig. 3(b) and (c). Taking a closer look at Fig. 3(a), it is shown that the etched channel gradually becomes narrow toward the end with NPs. We think that NPs continuously becomes small due to the reduction by C of graphene layer.

Fig. 3(a) exhibits that monolayer graphene on the right side was etched irregularly, and the etched edge was marked with a dotted line. Different from previous studies on graphene etching *via* carbon hydrogenation, a regular shape in the etched structures was not found in any microscopic analysis of this study. It can be attributed to the number of graphene layer and the surface roughness of silicon oxide layer. It has been reported that ZnO NPs do not move to crystallographic direction on graphite during carbon gasification reaction.[31] Furthermore, catalytic etching of single layer graphene is influenced by substrate morphology, leading to irregular nano- pattern.[37]

This journal is © The Royal Society of Chemistry 2012
Physical Chemistry Chemical Physics Accepted Manuscript

Table 1 Area ratio of C 1s component before and after etching graphene sheet.

Component	Concentration [%]	
	Before etching	After etching
vacancy defect	0.0	37.6
sp^2-hybridized carbon	71.0	34.4
sp^3-hybridized carbon	14.7	22.2
C-O	9.1	2.5
C=O	5.2	3.3

XPS analysis

X-ray photoelectron spectroscopy (XPS) analysis can clarify a change of sp^2-hybridized carbon into other states and oxidation state of Zn element. Hence, to investigate the valence state of C and Zn element, XPS analysis was conducted on the surface of graphene in the channel of FETs before and after the whole etching process. Fig. 4(a) shows the wide scan of XPS spectra obtained from the fully etched graphene by ZnO. As seen in the figure, peaks corresponding to C, O and Zn elements appear in the wide scan, but N element was not detected. It means that the precursor was totally transformed into metal oxide through thermal calcination to form ZnO NPs on graphene. The strong peak of O 1s could be attributed to oxygen originated from the SiO_2 as a dielectric layer of the FETs, or partially to ZnO NPs. To clarify the valence state of Zn element, core level spectra were also obtained from monolayer graphene after etching. Fig. 4(b) represents the core level spectra of Zn 2p after etching graphene under Ar atmosphere. Two major peaks are observed at the binding energy of 1022 and 1045.1 eV which are corresponding to Zn $2p_{3/2}$ and Zn $2p_{1/2}$, respectively. According to the NIST Standard Reference Database, these binding energies correspond to the values of Zn and ZnO.[38] Because of this ambiguity, the value of spin orbit splitting is normally used to distinguish the oxidation state between ZnO and Zn. The value of spin orbit splitting in Fig. 4(b) was 23.1 eV which is the same result reporting on the valence state of Zn metal.[39] This strongly means that carbon oxidation by ZnO NPs successfully occurred at 250 °C under Ar atmosphere, leading to etched structures on monolayer graphene. In Fig. 4(b), a shoulder is seen at the binding energy of 1021 and 1044 eV so that deconvolution was performed on two spectra corresponding to Zn $2p_{3/2}$ and Zn $2p_{1/2}$. The difference between those binding energies is 23.0 eV which corresponds to the same value obtained from ZnO.[39] This means that Zn element partially exists in the form of ZnO. Therefore, it is thought that the exposure of reduced ZnO to air is significant in order to obtain in the form of oxidation state.

Comparing XPS spectra of C 1s before and after etching clarifies a difference between sp^2-hybridized carbon and disordered carbons such as sp^3-hybridized carbon or vacancy defect in a honeycomb structure. Fig. 4(c) and (d) present the core level spectra of C 1s before and after carbon oxidation by ZnO. The binding energy of C 1s spectra was calibrated to 284.6 eV. Fig. 4(d) reveals that the shoulders appear at C 1s spectra after etching graphene.

For more detailed information, the core level spectra of C 1s were deconvoluted into five Gaussian peaks which were centered at 284.3, 284.6, 285.6, 286.7 and 288.9 eV. Those binding energies can be assigned to carbon vacancy, sp^2-hybridized carbon, sp^3-hybridized carbon, C-O and C=O, respectively.[40,41] Table 1 summarizes the area ratio of each deconvoluted component before and after etching. As shown in the table, the area of sp^2 component decreased from 71.0 to 34.4% after etching. On the other hand, the etching produced vacancy component of which area is about 37.6% after the solid-state reaction finished. The area of vacancy defect before etching is nearly zero in spite of the deconvolution. The components of C-O and C=O decreased down to 2.5 and 3.3%, implying that the oxygen was removed by heat treatment under Ar atmosphere or transformed into CO or CO_2 by the etching process. Interestingly, sp^3 component increased 1.5 times up to 22.2% by heat treatment for etching. Here, the participation of oxygen in the reaction can be excluded because the reaction occurred under Ar atmosphere. This strongly suggests that the dangling bond, which was created by catalytic etching,[40] and ZnO decoration mainly contributed to the increase of sp^3 component.[42] These results mean that carbon atoms in the graphene could be etched, resulting in breaking the symmetry of sp^2-hybridized and vacancy carbon atoms.

Raman spectroscopy analysis

Raman spectroscopy is used to clearly confirm the numbers of graphene layers and to quantify the degree of sp^2-hybridized carbon on graphene sheet.[43] G-band spectra around 1580 cm^{-1} are related to sp^2-hybridized carbon while D-band around 1350 cm^{-1} is associated with defects or disorder in graphene. In addition, 2D-band spectra show up around 2700 cm^{-1} as overtone of D-band. In general, R-value is defined as the intensity ratio of D-band to G-band spectra and this enables to estimate and quantify the defectiveness of graphene. Moreover, the intensity ratio of G-and 2D-band gives the information about the number of layer in graphene sheet. Fig. 5 displays Raman spectra of pristine and fully etched graphene. The figure clearly indicates that the intensity ratio of G-band to 2D-band is 0.5 which is a feature shown in monolayer graphene.[43] This means that monolayer graphene was successfully grown in Ge substrate and transferred to the SiO_2/Si substrate. The D-band shown in pristine graphene could be attributed to the grain boundaries formed during graphene growth.[44,45] The other possibility is the presence of oxygen on pristine graphene as shown in XPS analysis. Fig. 5

Physical Chemistry Chemical Physics Accepted Manuscript

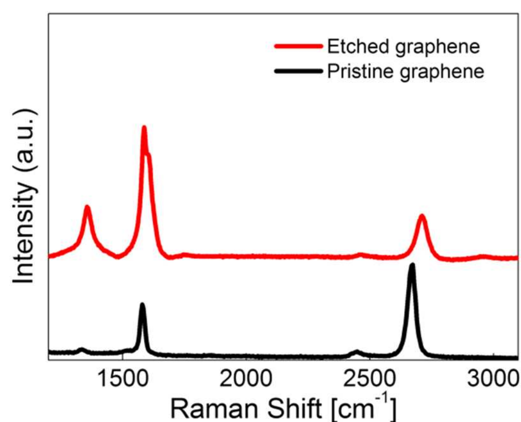

Fig. 5 Raman spectra of pristine and fully etched monolayer graphene. R-value increased from 0.07 to 0.36 after etching processes.

indicates that R-value increased from 0.07 to 0.36 after etching processes. In addition, D´-band, which is also related to defect of graphene, and G-band spectra are merged after the solid-state reaction finished. This strongly means that the density of defect increased dramatically in monolayer graphene sheet.[46,47] Commonly, it has been reported that the full width at half maximum (FWHM) of G-band became broad when the symmetry in honeycomb structure was broken and that graphene was converted to amorphous carbon when FWHM has the value of 200-300 cm^{-1}.[48,49] The FWHM of G-band in Fig.5 still has the value less than 100 cm^{-1} even after etching graphene fully. This indicates that monolayer graphene still keeps crystallinity rather than amorphous carbon.

I-V characteristics with percolation theory

To monitor the evolution of etching on monolayer graphene, current-voltage characteristics were measured from the FETs after every etching process. Fig. 6 shows the plot of conductance of graphene sheet versus the number of catalytic etching. Unexpectedly, the conductance of graphene decreased after heat treatment at 250 °C under Ar atmosphere to form ZnO NPs from the precursor. It can be attributed to the vacancy creation by the solid-state reaction between ZnO and C. It has been reported that $Zn(NO_3)_2 \cdot 6H_2O$ starts to be decomposed into ZnO from 150 to 250 °C under inert gas atmosphere ($Zn(NO_3)_2 \rightarrow ZnO + NO_x$).[50] It is thought that the precursor was thermally decomposed into ZnO NPs during decoration process. Therefore, it is inferred that graphene was partially etched by ZnO NPs which was formed below 250 °C ($ZnO + C \rightarrow Zn + CO$ or CO_2). As etching proceeds successively, the conductance of FETs exponentially decreases from 79 mS to 8 μS. It is out of question that monolayer graphene was etched by the solid-state reaction between ZnO and C despite the reaction occurred under Ar atmosphere. Fig. 6(b) reveals that the decrease of normalized transconductance represents the same tendency as conductance shows in Fig. 6(a), meaning that gate dependence

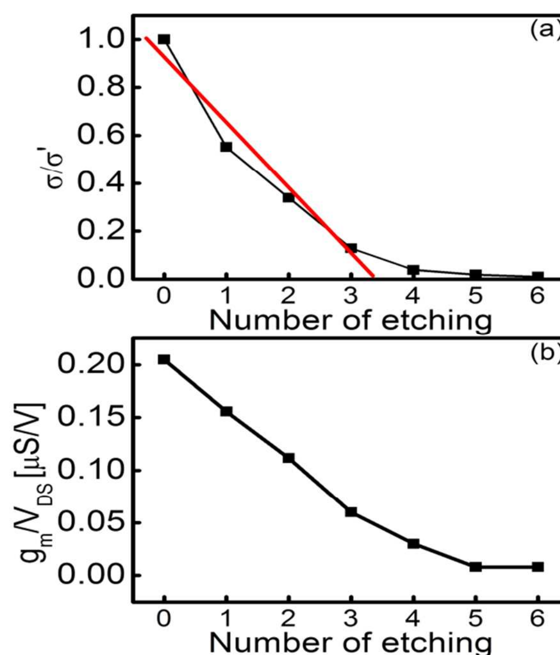

Fig. 6 (a) Normalized conductance as a function of the number of etching. The data were fitted to a line (red) to obtain critical exponent. (b) Normalized transconductance (g_m/V_{DS}) as a function of the number of etching at V_{DS} = 500 mV.

is hardly influenced by etching monolayer graphene. It can be explained that as shown in SEM images, the area of monolayer graphene is still relatively large in spite of carbon vacancies by a series of etching process.

The trend in conductance variation is similar to percolation phenomena in a two-dimensional film. According to the previous works, the gradual decline in conductance was analyzed by bond percolation.[51,52] Therefore, the diminishment of conductance can be interpreted by bond percolation theory in honeycomb structure. In this study, the relationship between conductance and carbon vacancy can be expressed as the following equation:

$$\frac{\sigma}{\sigma'} \propto (P_C - P)^t$$

where, σ, σ´, P_C, P and t are conductance, conductance before chemical reaction, the fraction of carbon vacancy at σ = 0, the fraction of carbon vacancy, and critical exponent, respectively. It was generally known that the critical exponent is calculated to be 1.27-1.45 in the case of bonding percolation in honeycomb lattice which represents graphene structure quite well.[53] In order to extract t, σ / σ´ is plotted as a function of the number of etching in Fig. 6(a), and the first four data were used to find an optimal value of t. This is because conductance approaches to almost zero after four in the axis of the number of etching. The optimal t was determined by selecting R-square value which is close to 1 in parameter fitting and the

Physical Chemistry Chemical Physics Accepted Manuscript

This journal is © The Royal Society of Chemistry 2012

Table 2 R-square values with respect to fitted critical exponent.

Critical exponent (t)	R-square
1.1	0.95
1.2	0.96
1.3	0.97
1.4	0.98

results are summarized in Table 2. The table indicates that an optimal value is found at $t = 1.4$ where R-square value almost approaches to 1. This value falls in the range of 1.27-1.45, meaning that conductance variation of graphene by catalytic etching obeys two dimensional bonding percolation theory in honeycomb structure. Therefore, it is certain that the axis of the number of etching comprehends (P_C - P) mathematically. Consequently, it reveals that the gradual evolution of vacancy defect in monolayer graphene decreases its conductance according to the bond percolation theory in honeycomb structure.

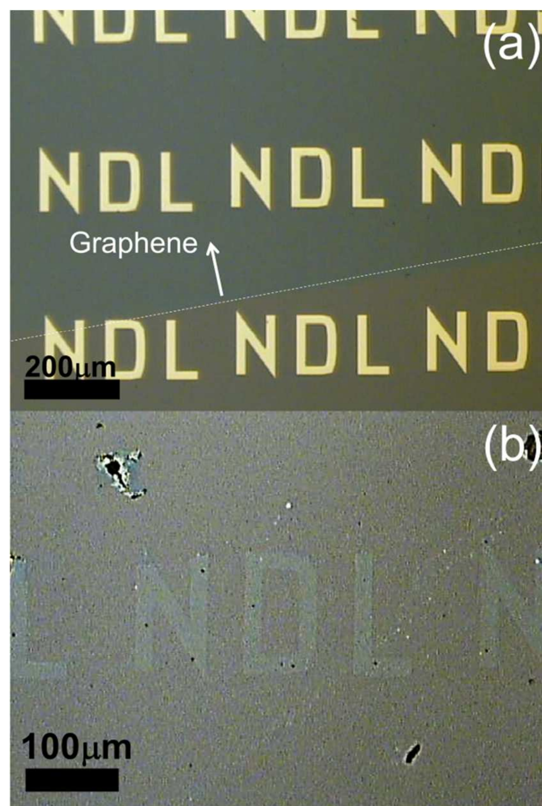

Fig. 7 (a) Metal mask deposited on monolayer graphene for patterning. Dotted line was put at the edge of monolayer graphene on SiO_2/Si substrate. (b) Patterned monolayer graphene by carbon gasification in air.

Finally, in order to demonstrate the usefulness of catalytic etching by carbon oxidation, monolayer graphene was patterned by using ZnO NPs. Fig. 7(a) displays monolayer graphene with Al mask on SiO_2/Si substrate, where a dotted line is marked at the edge of graphene. The Al-masked samples w ere oxidized in air at 300 °C for 2 h with ZnO catalyst to accelerate the catalytic reaction of etching process. Then, the substrate with patterned graphene was dipped in deionized water to remove unmasked graphene on SiO_2/Si substrate. Fig. 7(b) exhibits an optical image of well-patterned monolayer graphene after etching. This shows that graphene can be patterned to various shapes by changing a design of metal mask.

Conclusions

In conclusion, it was demonstrated that graphene can be etched at low temperature by using catalytic carbon gasification. Morphological information of etched graphene was obtained by using SEM, and AFM analysis. It revealed that after the solid-state reaction between ZnO and C was over, monolayer graphene had a lot of etched structures in the shape of pits and channels (reduction: $ZnO + C \rightarrow Zn + CO$ or CO_2, oxidation: $Zn + 1/2O_2 \rightarrow ZnO$). XPS analysis confirmed the presence of ZnO and Zn metal, and strongly supported that ZnO NPs were involved in the etching of carbon gasification. Raman spectra also showed that the degree of defects increased with the repetition of the catalytic etching. The evolution of vacancies was confirmed by monitoring the conductance of graphene after each step of catalytic etching. In addition, the conductance of etched graphene was analyzed with percolation theory in honeycomb structure. As a result, the experimental value of critical exponent is 1.4 which is close to theoretical value. Finally, pattern of etched graphene was successfully obtained by heating Al-masked graphene under air atmosphere in the presence of ZnO NPs. Also, this work highlights the possibility of destroying the honeycomb structure when graphene is exposed to heat with metal or metal oxide impurities from Cu or Ni foil.

Experimental

Synthesis of monolayer graphene and FETs fabrication

Monolayer graphene was synthesized on poly-crystalline Ge substrate by a CVD method described in ref. 54, 55. In the process of transfer, dry transfer method using thin metal film was employed to prevent organic contamination.[55] The graphene sheet was transferred on a heavily p-doped silicon substrate with 300 nm SiO_2 so that the back gate can be available. Pt with a thickness of 100 nm was deposited as source/drain contacts by using metal masks to avoid impurity contamination.

Etching process of graphene with ZnO

$Zn(NO_3)_2 \cdot 6H_2O$ (Aldrich, 98%) was adapted as a precursor to decorate monolayer graphene with ZnO NPs. 6 and 50 mg of

Physical Chemistry Chemical Physics Accepted Manuscript

$Zn(NO_3)_2\cdot 6H_2O$ were added in 20 ml of ethanol to prepare low (1 mM) and high (8 mM) concentration solutions. The solutions were sonicated for 15 min to dissolve the precursor totally. Then, 2 (low concentration) and 15 μl (high concentration) of the precursor solutions were separately dropped on monolayer graphenes at the channel of FETs. Next, the devices were dried at room temperature until ethanol was evaporated thoroughly. To decorate graphene with ZnO NPs, the FETs were heated in a furnace at 250 °C for 2 h under Ar atmosphere. In order to etch graphene sheet on FETs, additional heat treatment was conducted several times like following method: graphene with ZnO NPs was exposed to air for one night at room temperature and heated under the same condition to etch graphene by the solid-sate reaction between C and ZnO ($ZnO + C \rightarrow Zn + CO$ or CO_2). After this treatment, the devices were again stagnated in air for one night for the reduced Zn to be oxidized ($Zn + 1/2O_2 \rightarrow ZnO$) and heated again at 250 °C for 2 h under Ar atmosphere to further develop the etched structures on graphene sheet. This process was repeated 5 times to develop the etched structures.

Characterization of the etched graphene

The morphological change of graphene was observed after etching by optical microscope (OLYMPUS, BX41M and U-CMAD3) and scanning electron microscope (TESCAN, MIRA 3 FEG SEM). For more specific information, atomic force microscope (Park Systems, Park XE100) was also conducted to examine etched structure of monolayer graphene and the distribution of ZnO NPs. X-ray photoelectron spectroscopy analysis (Ulvac-PHI, PHI 5000 VersaProbe) was carried out to investigate the oxidation state of C and Zn elements before and after etching process. Raman spectroscopy (HORIBA JOBIN YVON, HR800-UV) using Ar laser excitation 514.5 nm was employed to study the degree of defectiveness. To characterize the electrical properties of graphene on FETs by vacancy evolution, current-voltage characteristics were measured by semiconducting parameter analyzer (Agilent, 4155C) after each etching process.

Patterning of monolayer graphene

Monolayer graphene was transferred to SiO_2/Si substrate, and Al (thickness: 20 nm) was deposited on graphene as a mask to protect the masked region of graphene. Next, the sample was heated at 300 °C for 2 h in air after dropping precursor solution on the masked graphene. After the solid-state reaction for etching were completed, the sample was dipped into deionized water and then dipped in tetramethyl ammonium hydroxide 3 wt.% solution to remove other graphene pieces and Al mask. Finally, well-patterned graphene was formed on the SiO_2/Si substrate.

Acknowledgements

This work is supported by the second stage of the Brain Korea 21 Plus Project in 2014.

Notes and references

[a] School of Electrical Engineering, Korea University, Anam-dong, Seongbuk-gu, 136-713 Seoul, Korea. E-mail: nanotube@korea.ac.kr, gtkim@korea.ac.kr; Tel: +82-2-3290-3801
[b] School of Advanced Materials Science and Engineering, Sungkyunkwan University, 300 Cheoncheon, Jangan-gu, Suwon 440-746, Korea

1 R. R. Nair, P. Blake, A. N. Grigorenko, K. S. Novoselov, T. J. Booth, T. Stauber, N. M. R. Peres, A. K. Geim, *Science*, 2008, **320**, 1308.
2 K. S. Kim, Y. Zhao, H. Jang, S. Y. Lee, J. M. Kim, K. S. Kim, J.-H. Ahn, P. Kim, J.-Y. Choi, B. H. Hong, *Nature*, 2009, **457**, 706-710.
3 C. Lee, X. Wei, J. W. Kysar, J. Hone, *Science*, 2008, **321**, 385-388.
4 A. A. Balandin, S. Ghosh, W. Bao, I. Calizo, D. Teweldebrhan, F. Miao, C. N. Lau, *Nano Lett.*, 2008, **8**, 902-907.
5 K. S. Novoselov, A. K. Geim, S. V. Morozov, D. Jiang, Y. Zhang, S. V. Dubonos, I. V. Grigorieva, A. A. Firsov, *Science*, 2004, **306**, 666-669.
6 Y. Zhang, Y.-W. Tan, H. L. Stormer, P. Kim, *Nature*, 2005, **438**, 201-204.
7 X. Wang, L. Zhi, K. Mullen, *Nano Lett.*, 2008, **8**, 323-327.
8 X. Li, H. Zhu, K. Wang, A. Cao, J. Wei, C. Li, Y. Jia, Z. Li, X. Li, D. Wu, *Adv. Mater.*, 2010, **22**, 2743-2748.
9 J. Wu, M. Agrawal, H. A. Becerril, Z. Bao, Z. Liu, Y. Chen, P. Peumans, *ACS Nano*, 2010, **4**, 43-48.
10 J. Meyer, P. R. Kidambi, B. C. Bayer, C. Weijtens, A. Kuhn, A. Centeno, A. Pesquera, A. Zurutuza, J. Robertson, S. Hofmann, *Sci. Rep.*, 2014, **4**, 5380.
11 I.-Y. Lee, H.-Y. Park, J.-H. Park, G. Yoo, M.-H. Lim, J. Park, S. Rathi, W.-S. Jung, J. Kim, S.-W. Kim, Y. Roh, G.-H. Kim, J.-H. Park, *Nanoscale*, 2014, **6**, 3830-3836.
12 Y. Wang, L. Wang, T. Yang, X. Li, X. Zang, M. Zhu, K. Wang, D. Wu, H. Zhu, *Adv. Funct. Mater.*, 2014, **24**, 4666-4760.
13 K. Carva, B. Sanyal, J. Fransson, O. Eriksson, *Phys. Rev. B*, 2010, **81**, 245405.
14 J. J. Palacios, J. Fernandez-Rossier, L. Brey, *Phys. Rev. B*, 2008, **77**, 195428.
15 C. S. Park, Y. Zhao, J.-H. Lee, D. Whang, Y. Shon, Y.-H. Song, C. J. Lee, *Appl. Phys. Lett.*, 2013, **102**, 032106.
16 M. Y. Han, B. Ozyilmaz, Y. Zhang, P. Kim, *Phys. Rev. Lett.*, 2007, **98**, 206805.
17 L. Jiao, L. Zhang, X. Wang, G. Diankov, H. Dai, *Nature*, 2009, **458**, 877-880.
18 F. Guinea, M. I. Katsnelson, M. A. H. Vozmediano, *Phys. Rev. B*, 2008, **77**, 075422.
19 J. Bai, X. Zhong, S. Jiang, Y. Huang, X. Duan, *Nat. Nanotechnol.*, 2010, **5**, 190-194.
20 D. V. Kosynkin, A. L. Higginbotham, A. Sinitskii, J. R. Lomeda, A. Dimiev, B. K. Price, J. M. Tour, *Nature*, 2009, **458**, 872-876.
21 A. L. Elías, A. R. Botello-Méndez, D. Meneses-Rodríguez, V. J. González, D. Ramírez-González, L. Ci, E. Muñoz-Sandoval, P. M. Ajayan, H. Terrones, M. Terrones, *Nano Lett.*, 2010, **10**, 366–372.
22 J. Wang, L. Ma, Q. Yuan, L. Zhu, F. Ding, *Angew. Chem. Int. Ed.*, 2011, **50**, 8041–8045.

Physical Chemistry Chemical Physics Accepted Manuscript

This journal is © The Royal Society of Chemistry 2012

23 S. Fujii, T. Enoki, *J. Am. Chem. Soc.*, 2010, **132**, 10034–10041.
24 L. Ma, J. Wang, F. Ding, *Angew. Chem. Int. Ed.*, 2012, **51**, 1161–1164.
25 L. Ci, L. Song, D. Jariwala, A. L. Elias, W. Gao, M. Terrones, P. M. Ajayan, *Adv. Mater.*, 2009, **21**, 4487-4491.
26 S. S. Datta, D. R. Strachan, S. M. Khamis, A. T. C. Johnson, *Nano Lett.*, 2008, **8**, 1912-1915.
27 L. Ma, J. Wang, J. Yip, F. Ding, J. Phys. *Chem. Lett.*, 2014, **5**, 1192-1197.
28 W. Baaziz, G. Melinte, O. Ersen, C. Pham-Huua, I. Janowska, *Phys. Chem. Chem. Phys.,* 2014, **16**, 15988-15993
29 L. Gao, W. Ren, B. Liu, Z.-S. Wu, C. Jiang, H.-M. Cheng, *J. Am. Chem. Soc.* 2009, **131**, 13934–13936.
30 L. Zhang, S. Diao, Y. Nie, K. Yan, N. Liu, B. Dai, Q. Xie, A. Reina, J. Kong, Z. Liu, *J. Am. Chem. Soc.* 2011, **133**, 2706–2713
31 D. W. McKee, *Carbon*, 1970, **8**, 623-635.
32 Z. J. Pan, R. T. Yang, *J. Catal.*, 1991, **130**, 161-172.
33 X. X. Wang, J. N. Wang, L. F. Su, J. J. Niu, *J. Mater.*, Chem. 2006, **16**, 4231-4234.
34 D.-H. Kim, K. Waki, *J. Nanosci. Nanotechno.*, 2010, **10**, 2375-2380.
35 S. Y. Lee, D.-H. Kim, S. C. Choi, D.-J. Lee, J. Y. Choi, H.-D. Kim, *Micropor. Mesopor. Mat.*, 2014, **194**, 46-51.
36 W. L. Holstein, M. Boudart, *Fuel*, 1983, **62**, 162-165.
37 T. Tsukamoto, T. Ogino, *J. Phys. Chem. C*, 2011, **115**, 8580-8585.
38 NIST X-ray Photoelectron Spectroscopy Database, Version 4.1 (National Institute of Standards and Technology, Gaithersburg, 2012)
39 C. Wagner, G. Muilenberg, Handbook of X-ray photoelectron spectroscopy, Perkin-Elmer, 1979, p. 84.
40 H. Estrade-Szwarckopf, *Carbon*, 2004, **42**, 1713-1721.
41 A. Barinov, O. B. Malcioglu, S. Fabris, T. Sun, L. Gregoratti, M. Dalmiglio, M. Kiskinova, *J. Phys. Chem. C*, 2009, **113**, 9009-9013.
42 A. Velamakanni, C. W. Magnuson, K. J. Ganesh, Y. Zhu, J. An, P. J. Ferreira, R. S. Ruoff, *ACS Nano*, 2010, **4**, 540-546.
43 A. C. Ferrari, J. C. Meyer, V. Scardaci, C. Casiraghi, M. Lazzeri, F. Mauri, S. Piscanec, D. Jiang, K. S. Novoselov, S. Roth, A. K. Geim, *Phys. Rev. Lett.*, 2006, **97**, 187401.
44 I. Vlassiouk, M. Regmi, P. Fulvio, S. Dai, P. Datskos, G. Eres, S. Smirnov, *ACS Nano*, 2011, **5**, 6069-6076.
45 X. Li, C. W. Magnuson, A. Venugopal, J. An, J. W. Suk, B. Han, M. Borysiak, W. Cai, A. Velamakanni, Y. Zhu, L. Fu, E. M. Vogel, E. Voelkl, L. Colombo, R. S. Ruoff, *Nano Lett.*, 2010, **10**, 4328.
46 L. G. Cancado, A. Jorio, E. H. Martins Ferreira, F. Stavale, C. A. Achete, R. B. Capaz, M. V. O. Moutinho, A. Lombardo, T. S. Kulmala, A. C. Ferrari, *Nano Lett.*, 2011, **11**, 3190-3196.
47 M. M. Lucchese, F. Stavale, E. H. Martins. Ferreira, C. Vilani, M. V. O. Moutinho, R. B. Capaz, C. A. Achete, A. Jorio, *Carbon*, 2010, **48**, 1592-1597.
48 A. C. Ferrari, J. Robertson, *Phys. Rev. B*, 2000, **61**, 14095.
49 A. C. Ferrari, J. Robertson, *Phys. Rev. B*, 2001, **64**, 075414.
50 J. Chen, Z. Feng, P. Ying, M. Li, B. Han, C. Li, *Phys. Chem. Chem. Phys.*, 2004, **6**, 4473-4479.
51 B. J. Last, D. J. Thouless, *Phys. Rev. Lett.*, 1971, **27**, 1719.
52 M. Sahimi, B. D. Hughes, L. E. Scriven, H. T. Davis, *J. Phys. C: Solid State Phys.*, 1983, **16**, L521-L527.
53 E. E. Vogel, W. Lebrecht, J. F. Valdes, *Physica A*, 2010, **389**, 1512-1520.
54 G. Wang, M. Zhang, Y. Zhu, G. Ding, D. Jiang, Q. Guo, S. Liu, X. Xie, P. K. Chu, Z. Di, X. Wang, *Sci. Rep.*, 2013, **3**, 2465.
55 J.-H. Lee, E. K. Lee, W.-J. Joo, Y. Jang, B.-S. Kim, J. Y. Lim, S.-H. Choi, S. J. Ahn, J. R. Ahn, M.-H. Park, C.-W. Yang, B. L. Choi, S.-W. Hwang, D. Whang, *Science*, 2014, **344**, 286-289.

Physical Chemistry Chemical Physics Accepted Manuscript